Journal of Thermal Science Vol.29, No.4 (2020) 955–971

https://doi.org/10.1007/s11630-020-1233-2 **Article ID: 1003-2169(2020)04-0955-17**

Investigation of the Conjugate Heat Transfer and Flow Field for a Flat Plate with Combined Film and Impingement Cooling

FU Jinglun[1,2*], CAO Ying[1,2], ZHANG Chao[3*], ZHU Junqiang[1,2]

1. Institute of Engineering Thermophysics, Chinese Academy of Sciences, Beijing 100190, China
2. University of Chinese Academy of Sciences, Beijing 100049, China
3. Tianjin Key Laboratory for Advanced Mechatronic System Design and Intelligent Control, Tianjin 300384, China

Abstract: Film cooling combined with internal impingement cooling is one of the most effective technologies to protect the gas turbine vanes and blades from the hot gas. In this study, conjugate heat transfer CFD study was undertaken for a flat plate with combined film cooling and impingement cooling. An experiment on conjugate heat transfer of a flat plate with combined film and impingement cooling was performed to validate the code. Then the effects of several parameters including Biot number, blowing ratio, film hole shape and impingement hole diameter on the overall cooling effectiveness were numerically studied. The results show that for a specific combined cooling scheme and a given blowing ratio, the coolant potential can be reasonably allocated to the internal and the external cooling to achieve the overall cooling effectiveness. As the blowing ratio increases, the overall cooling effectiveness trends to reach a maximum value. For different film hole geometrical, the maximum values of the overall cooling effectiveness at high blowing ratio approximate to the same value. At a given mass flow rate of coolant, the increase of the impingement hole diameter leads to the reduction of the overall cooling effectiveness.

Keywords: conjugate heat transfer, combined film and impingement cooling, overall cooling effectiveness, Biot number, blowing ratio

1. Introduction

To pursue higher thermal efficiency and specific work of the gas turbine, turbine inlet temperature is gradually increased. It has been very significant and inevitable to protect the turbine vanes and blades from an environment with high temperature and high pressure. The modern gas turbine cooling design usually combines the external film cooling and the internal forced convection cooling to reduce the metal surface temperature. With the increase of the turbine inlet temperature, gas turbine requires more advanced cooling technologies.

Film cooling combined with internal impingement cooling is one of the most effective technologies to protect the gas turbine vanes and blades from the hot gas. But these two kinds of cooling schemes have been separately investigated in the previous studies. Kercher [1] documented more than a thousand papers' titles in the field of film-cooling from 1971 to 1996. The early researches on the film cooling show that, with the

Received: Feb 26, 2019
AE: TALER Jan

Corresponding author: FU Jinglun; E-mail: fujl@iet.cn
ZHANG Chao czhangxj@163.com

Nomenclature

Bi	Biot number	X	distance from the center of Hole 1 exit in the streamwise direction/mm
BR	Blowing ratio	Y	distance from the flat plate side wall in the lateral direction/mm
D_i	diameter of the impinging hole/mm	y^+	dimensionless distance from the wall
d	diameter of the film cooling hole/mm	**Greek symbols**	
h_c	local convective heat transfer coefficient at the wall surface on the coolant flow side/W·m^{-2}·K^{-1}	δ	thickness of the film cooling plate
h_f	local convective heat transfer coefficient at the wall surface on the main flow side/W·m^{-2}·K^{-1}	ε	dissipation rate
$\bar{h}$	average convective heat transfer coefficient over the surface/W·m^{-2}·K^{-1}	κ	turbulent kinetic energy/m^2·s^{-2}
k	thermal conductivity/W·m^{-1}·K^{-1}	λ	thermal conductivity of the film cooling plate
M_i	coolant mass flow rate passing through the impingement cooling holes/kg·s^{-1}	μ	kinematic viscosity/m^2·s^{-1}
M_m	mainstream mass flow rate/kg·s^{-1}	ω	specific dissipation rate/s^{-1}
p	pitch of film holes/mm	ρ_c	coolant density/kg·m^{-3}
Re_i	impingement jet Reynolds number	ρ_i	coolant density passing through the impingement holes/kg·m^{-3}
T_c	coolant temperature/K	ρ_m	mainstream density of the main stream /kg·m^{-3}
T_m	mainstream air temperature/K	Φ	overall cooling effectiveness
$T_{w,e}$	temperature of the conjugate interface wall on the hot gas side/K	**Subscripts**	
$T_{w,i}$	temperature of the conjugate interface wall on the coolant side/K	c	coolant
V_c	coolant velocity passing through the film holes/ m·s^{-1}	i	impingement holes
V_i	average coolant velocity passing through the impingement holes	m	mainstream
V_m	mianstream velocity/m·s^{-1}	w	conjugate interface wall on the hot gas side

increase of the blowing ratio, the coolant ejected from a cylinder hole lifts off from the wall by a pair of kidney-shaped vortex in the downstream of the hole, which results in adiabatic film cooling effectiveness lowering. Bunker [2], Ekkad and Han [3, 4] catalogued the researches and data in the literatures and summarized the shaping geometries parameter ranges for film cooling. Many studies [5−11] indicated that shaped holes with expanded exits could greatly reduce the intensity of the kidney-shaped vortex pair, and further improve the adiabatic film cooling effectiveness. Taken the metal heat conduction into consider, Bohn et al. [12] compared adiabatic and overall cooling effectiveness for a flat pate with one row of film cooling holes by performing conjugate computation. They found that the overall cooling effectiveness was relatively more uniform compared with the adiabatic cooling effectiveness. In a similar study, Silieti et al. [13] reported that laterally averaged overall cooling effectiveness was significantly higher than the laterally averaged adiabatic cooling effectiveness. Liu et al. [14] compared the overall cooling effects of three typical film holes (cylindrical hole, shaped hole, and double-jet hole) by using the multi-field coupling method and pointed out that the net film cooling effectiveness under aero-thermal coupled condition is generally lower than that under adiabatic wall condition. Zhang et al. [15] obtained the correlation between overall cooling effectiveness and Biot number for the typical cylindrical film cooling holes on flat plate by performing conjugate heat transfer simulation.

For impingement cooling, the near wall flow characteristic and the heat transfer at the target wall of a single axisymmetric impinging jet has been revealed by several earlier studies [16−19]. In practice, multiple jets used in many cooling design result in a cross flow. Excessive cross flow can cause the downstream jets to be swept away from the target impingement surface, leading to a degradation of the overall surface convective heat

transfer [20]. By the studies of the jet impingement heat transfer characteristics, Downs and James [21], Viskanta [22] and Cho et al. [23] concluded that the influencing factors include the flow structure of the jet impingement, jet temperature, interaction between the coolant and the cross-flow, turbulence intensity and impingement hole shape. Goodro et al. [24−26] presented a comprehensive investigation on the effect of Reynolds number, Mach number, hole to target plate distance, hole spacing and temperature ratio on the heat transfer coefficients of an impingement array. They recommended that optimum jet to target plate distance varied between 1.5 and 3 for different Reynolds numbers.

Actually, the combined cooling effects involve the internal forced convection, external film convective heat transfer, and the heat conduction in the metal. It is necessary to apply conjugate heat transfer models to get the overall cooling effectiveness to evaluate the cooling performance for the scheme combined film cooling and internal impingement cooling. There are some studies based on conjugate heat transfer method for a configuration including internal impingement jets and film cooling. Sweeney and Rhodes [27] experimentally simulated a conjugate surface with a typical engine Biot number under blowing ratios of 0.7 to 1.5. Their results showed that impingement cooling dominated over film cooling in the influence on overall cooling effectiveness. Panda and Prasad [28, 29] conducted computational and experimental investigations on a flat plate combined impingement and film cooling. They concluded that the improvement on the overall cooling effectiveness from adding internal impingement became more substantial as the blowing ratio increased from 0.6 to 1.6. Maikell et al. [30] got the similar conclusion by measuring the overall cooling effectiveness in the stagnation region with impingement and round film-cooling holes at the leading edge region. The same leading edge model with shaped film-cooling holes and impingement was considered by Mouzon et al. [31] and Ravelli et al. [32]. But they found that the presence of impingement with hole height-diameter ratios higher than 5 had no obvious effect on the overall cooling effectiveness. Nathan et al. [33] performed the experiments on the leading edge of a scaled C3X vane under a blowing ratio range of 1.0 to 3.0 and a density ratio of 1.2. They found that impingement cooling was helpful for the improvement on the overall cooling effectiveness, and poor cooling effectiveness region existed due to the low film cooling effectiveness. Mensch et al. [34−36] experimentally and numerically investigated the overall cooling effectiveness over the endwall surface with jet impingement and film cooling under three blowing rates of 0.6, 1.0 and 2.0. They found that the contribution of the impingement cooling became stronger when the blowing ratio was 2.0. And Thermal Barrier Coating (TBC) reduced the equivalent solid thermal conductivity resulting in the increase of the overall cooling performance. Mensch [37] and Jung et al. [38] summarized that solid thermal conductivity affects the role of impingement in the combined cooling, either the jet impingement or the film cooling interact on each other. Though there are some researches focused on the investigation of the configuration combined both the impingement cooling and film cooling, there has been no systematic study so far to explain the different conclusions in the previous literatures. It is evidenced that the overall cooling effectiveness depends on internal cooling, external cooling and heat conduction of the metal. But the interaction mechanism between these three elements and the influence of them on the overall effectiveness is not totally understood and stated.

To put forth the understanding on the flow and thermal behavior of the scheme with internal and external cooling, the present paper will numerically investigate the effect of the Biot number, blowing ratio, the film and impingement hole geometries on the overall cooling effectiveness for the flat plates with combined film and impingement cooling configurations. After the introduction, the conjugate numerical simulation method are presented. The conjugate heat transfer experimental data of a flat plate is illustrated and used to validate the current numerical method. Then the effects of Biot number, the blowing ratio, film hole shape, impingement configurations are discussed in detail. The flow field, temperature and local heat transfer characteristics are analyzed in order to explain the behavior of the overall cooling performance. Finally, the paper ends with some conclusions.

2. Numerical Method

2.1 Computational domain and research objectives

In order to carry out the aero-thermal coupling calculations, the computational domain should include the mainstream and the coolant flow domain, as well as the solid metal domain. The whole computational domains for the flat plate with a single-row film cooling hole combined with the impingement cooling used in this paper are illustrated in Fig. 1. The size of the flow path for upper hot mainstream channel is 320 mm × 24 mm × 60 mm (length×width×height). The size of the lower coolant chamber is 180 mm × 24 mm × 6 mm (length× width×height).

The solid domains include the film cooling plate and the impingement cooling plate. The thickness of the film cooling plate is 12 mm (3*d*). A single row of film cooling holes is arranged through the film cooling plate. The circular hole and fan-shaped hole are chosen to

investigate the effects of the film hole geometric shape. The diameter of the circular film hole (d) is 4 mm. The incline angle α of the film cooling hole is 30° and the compound angle is 0°. The origin of the coordinates is located at the film hole exit on the main flow side. Axes X, Y and Z depict the stream-wise, lateral and height directions respectively. The fan-shaped hole is formed by expanding the cylindrical hole on both sides of the hole with an expansion angle of 14° as shown in Fig. 2. The

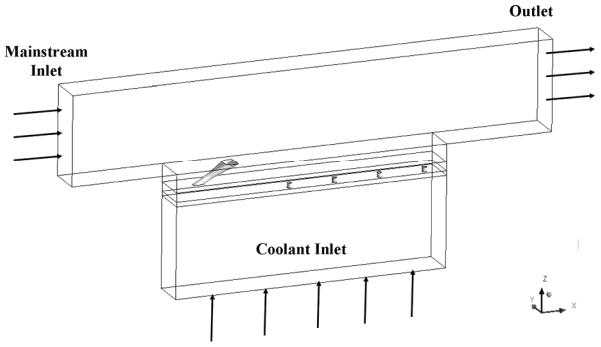

(a) 3D model of the computational domain

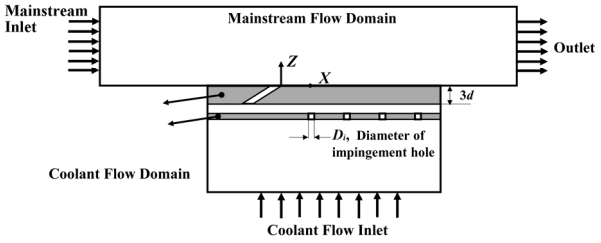

(b) X-Z cross section of cooling configuration

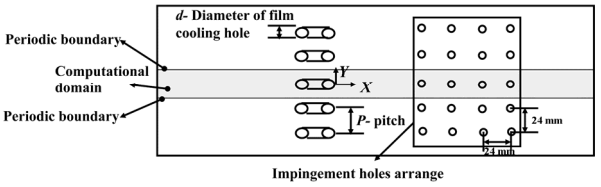

(c) Schematic of the flat plates with combined film and impingement cooling

Fig. 1 Computational domain of combined cooling configuration

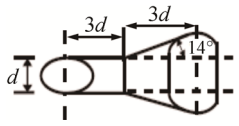

Fig. 2 Schematic of the fan shape film hole

distance between two film cooling holes in the lateral direction are 6d. The thickness of the flat plate with the impingement holes is 3 mm. The pitch between the two adjacent impingement holes in stream-wise direction is 24 mm. The distance in the stream-wise direction from the exit of the impingement holes to the entrance of the cooling holes is 10d. The jet-to-target plate spacing is 6 mm.

The main computing parameters and research objectives are listed in Table 1. The influences of Biot number, blowing ratio, film hole shape and impingement hole diameters are evaluated respectively.

Biot number (Bi) represents the ratio of the solid thermal resistance to the external convective heat transfer resistance, which is defined as follow:

$$Bi=\delta h/\lambda \tag{1}$$

where h is the external heat transfer coefficient on the mainstream flow side; δ is the thickness of the film cooling plate, and λ is the thermal conductivity of the film cooling plate. The values of Biot number are chosen as 0.022, 0.22 and 2.2 in this paper, which are calculated based on different material heat conductivity coefficient λ.

The blowing ratio (BR) is defined as following:

$$BR=\frac{\rho_c V_c}{\rho_m V_m} \tag{2}$$

where ρ_c is the density of the coolant; ρ_m is the density of the mainstream; V_c is the velocity of the coolant at the film hole exit, and V_m is the velocity of mainstream. In the present study, the blowing ratio varies from 0.5 to 3 to investigate the influence of the blowing ratio on overall cooling effectiveness.

The diameters (D_i) of the impingement holes are 3 mm and 6 mm respectively to investigate the effect of the impingement holes diameter.

Table 1 Computational model and research objectives

Research objectives	Biot number	Blow Ratio	Film hole shape	Jet-hole size
Effect of Biot number	0.022 0.22 2.2	1.0	Fan shaped film hole	3 mm
Effect of blowing ratio	0.22	0.5–3.0	Fan shaped film hole	3 mm
Effect of film cooling hole shape	0.22	0.5–3.0	Cylinder film hole Fan shaped film hole	3 mm
Effect of impingement hole diameter	0.22	1.0	Fan shaped film hole	3 mm 6 mm

The parameter to evaluate the cooling performance of the combined cooling scheme is overall cooling effectiveness (Φ), which is defined as follow:

$$\Phi = \frac{T_m - T_{w,e}}{T_m - T_c} \tag{3}$$

where Φ is the overall cooling effectiveness; $T_{w,e}$ is the temperature of the conjugate interface wall on the hot gas side; T_m and T_c are the inflow temperatures of the mainstream channel and coolant chamber respectively.

The heat transfer near the impingement target wall is evaluated by h_c, and the impingement Reynolds number is expressed as Re_i, and the definition of them can be written as following:

$$h_c = \frac{q}{T_{w,i} - T_c} \tag{4}$$

$$h_f = \frac{q}{T_m - T_{w,e}} \tag{5}$$

$$Re_i = \frac{D_i V_i}{\mu} \tag{6}$$

where q is the wall heat flux over the target wall surface; $T_{w,i}$ is the wall temperature of target surface; $T_{w,e}$ is the wall temperature of the external conjugate surface; μ is coolant kinematic viscosity and V_i is the velocity at the impingement hole.

2.2 Boundary condition

The finite volume based software package CFX is used for the aero-thermal coupling numerical simulations. The k-ω based Shear-Stress-Transport (SST) turbulence model is employed. The solution is considered to be converged when the root mean square of the residual value is in the order of 10^{-6} for continuity, momentum, turbulence quantities and for the energy equation. The discretization scheme is second-order accurate. All the computations are continued until the solid plate temperature has attained a steady state.

The coolant firstly impinges on the target surface, and then it is released from the film holes and mixed with the mainstream air in the mainstream channel. Hence, there is only one outlet of the whole fluid domain. At the mainstream flow inlet, flow direction (along with X axis), flow velocity (V_m=35 m/s), total temperature (T_m= 333.15 K) and turbulence intensity (5%) are specified. The outlet pressure is given as an ambient pressure. At the coolant chamber inlet, flow direction (along with the Z axis), flow velocity, total temperature (T_c=298.15 K) and turbulence intensity (5%) are also specified. The flow velocity at the coolant chamber inlet is adjusted to obtain the expected blowing ratio. The specified temperatures of the mainstream flow and coolant are kept consist with the values in the following experiment for validation.

The conjugate interface boundary conditions are imposed on all the fluid-solid interfaces of the target plate. The boundary conditions of the other solid walls of the jet plate are defined as non-slip, smooth and adiabatic wall.

2.3 Mesh and mesh independence

The structured meshes for both the fluid domain and the solid domain with the boundary layers are generated together by using the commercial software ICEM CFD. The grid nodes on either side of the fluid-solid interfaces are one-to-one correspondence to reduce the interpolation error. The meshes near the film holes and the impingement holes are refined to well resolve the flow and heat transfer in detail. The y^+ in the first cell adjacent to the wall is below 1 with respect to the criteria required for the individual near-wall treatment. The meshes used in the present study for fluid domain and solid domain are shown in Fig. 3.

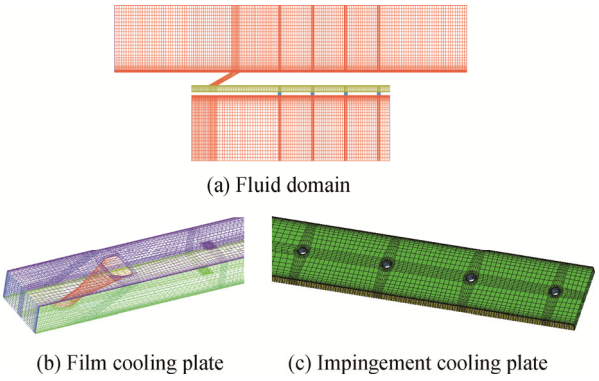

Fig. 3 Meshes for the fluid and solid domains

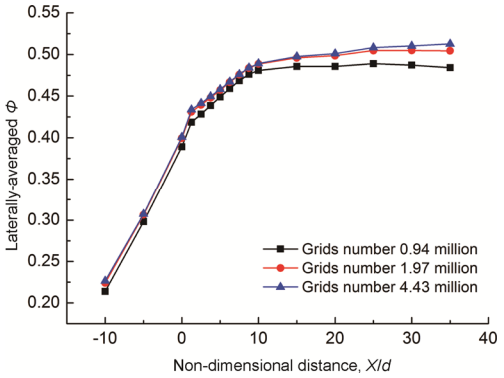

Fig. 4 Distribution of the laterally-averaged Φ for different grids numbers

Mesh independence validation is done for the fan-shaped film hole combined with jet impingement model. As shown in Fig. 4, the laterally-averaged overall cooling effectiveness is compared for three different meshes with 0.94 million, 1.97 million and 4.43 million. As the mesh

number increases from 1.97 million to 4.43 million, the values of laterally-averaged overall cooling effectiveness change little in the range of $-10<X/d<10$ (X/d represents non-dimensional stream-wise distance), and differ with 1% in the region of $X/d>10$. To balance the prediction accuracy and computational cost, the total mesh number is chosen around 1.97 million in the following simulations.

3. Code Validation

A conjugate heat transfer experiment was conducted on the flat-plate test rig to validate the current numerical code. The experiment was performed on a low speed wind tunnel at Institute of Engineering Thermophysics, Chinese Academy of Sciences. The test rig is an open loop continuously operating facility, as shown in Fig. 5.

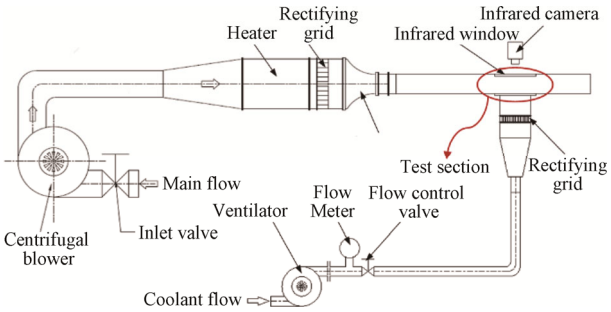

Fig. 5 Flat plate experimental sketch

The mainstream flow was provided by a 55 kW centrifugal blower. An electric duct heater was used to heat the mainstream flow to a required temperature of 333.15 K. Then, the flow passed through the screens, baffles, and a circular-to-square transition duct to the test section. With this conditioning, a two-dimensional flow uniformity of ±0.4% in terms of velocity was obtained for low free stream turbulence levels. The test section was made of Plexiglas and had a 0.4 m×0.09 m (W×H) square cross-section. The free stream velocity and temperature were measured through a pitot tube and a co-located T-type thermocouple. The uncertainty of the velocity measurements was within ±1.5%. The coolant was supplied using an air supply apparatus, which consisted of a low capability blower, a flow meter and a condition valve. The temperature of the coolant air varied from 298.15 to 299 K. An additional T-type thermo-couple was placed in the coolant chamber to measure the coolant temperature. The error of the thermocouple is ±0.2 K. The flat plate with film cooling hole was made of stainless steel AISI 304 with a thermal conductivity of 14.9 W/(m·K) obtained at the temperature of 303.15 K. The flat plate with impingement holes is made of aluminum. An infrared camera (VarioCAM hr head) was used to capture the surface temperature distribution of the test configuration on the mainstream flow side. The camera is capable of recording up to 400 frames per second with a 320×240 pixel image. The camera was installed 200 mm higher than the flat plate, as shown in Fig. 5. The infrared camera was calibrated before the experiment to correct the radiation-temperature curve [39]. The error of the camera is ±1 K. The uncertainty of the measured overall cooling effectiveness is ±7.22%–±9.63% when Φ equals to 0.4–0.3.

The tested cooling configuration was shown in Fig. 1(c). One row of film cooling holes and four rows of impingement cooling holes were arranged. There are totally 20 cylindrical impingement holes arranged in an array of 4×5. The pitch between the two adjacent impingement holes is 24 mm and the stream-wise distance of two rows of impingement holes is 24 mm.The geometrical dimensions of the test plate was the same with the relevant computational model.

The calculated laterally-averaged overall cooling effectiveness at BR=1.5 was compared with the experimental data, which is shown in Fig. 6. The numerical results and the experimental data agree well in terms of overall trend. The laterally-averaged overall cooling effectiveness increases along the stream-wise direction. But the values of the experiment data are a little lower than those of the numerical results especially at the region downstream of the film cooling hole. The reasons for the discrepancies may be caused by the different between the specified solid thermal conductivity and the real value. Nonetheless, the comparisons in Fig. 6 demonstrated the overall trend reliability of the CFD results.

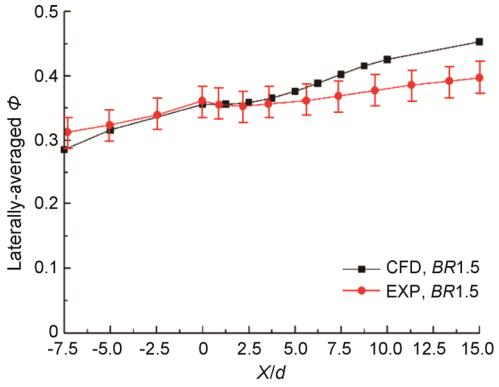

Fig. 6 Laterally-averaged overall cooling effectiveness distribution for BR=1.5

4. Results and Discussion

4.1 Effects of Biot number

The effect of Biot number on the overall cooling effectiveness, temperature and flow field characteristic was first investigated for the fan-shaped film cooling

hole at a fixed blowing ratio BR=1. In the present study, three Biot numbers with values of 0.022, 0.22 and 2.2 were obtained by altering the thermal conductivity of the conjugated film cooling plate. The thermal conductivities of film cooling plate and the corresponding Biot number are listed in Table 2. Note that, the medium Biot number with value of 0.22 is roughly equivalent to that of a real engine under typical working conditions [40]. As the blowing ratio is usually medium or high for the real vane and blade film cooling, the case of blowing ratio BR=1 was chosen for the comparisons among different Biot numbers.

Table 2 Thermal conductivity and the corresponding Biot number

Thermal conductivity coefficient k/W·m^{-1}·K^{-1}	1.1	11	110
Bi	2.2	0.22	0.022

The contours of overall cooling effectiveness on the wall surface of the main flow side at Bi=2.2, 0.22 and 0.022 are respectively shown in Fig. 7. It can be seen that Bi has a great impact on the overall cooling effectiveness (Φ) distributions at the same blowing ratio. For the case with a larger Bi value (i.e., Bi=2.2), the profile of Φ distribution is similar to that of an adiabatic film cooling on a plate, which implies the impingement cooling contributes little to Φ. For the case with a smaller Bi value (i.e., Bi=0.022), due to the high heat conduction of the film cooling plate, the upstream region of the film hole can be also well cooled. The distribution of overall cooling effectiveness exhibits more uniform both in stream-wise and lateral directions. For the case with the Bi value similar to the real engine, the contribution of the film cooling seems a little stronger than that of the impingement cooling in the region from the film hole exit to the downstream of X/d=10. While in the downstream region from X/d=10 to 35, the influence of the impingement cooling seems stronger.

The laterally-averaged overall cooling effectiveness distributions for the cases with different Bi on the wall surface of main flow side in the stream-wise direction are shown in Fig. 8. As mentioned above, the overall cooling effectiveness takes both film cooling effects on the main flow side and convention cooling effects on the coolant side into accounted. For a specific combined cooling scheme and the given flow conditions of main flow and coolant, the thermal conductivity (i.e. the Biot number) of the film cooling plate decides the contribution proportion of impingement cooling and film cooling to the overall cooling effectiveness. With Bi increasing, the role of the film cooling becomes more and more important. When the Biot number approaches to infinity under the adiabatic wall condition, the overall cooling effectiveness is equivalent to the adiabatic cooling effectiveness. With the value of Bi decreasing from 2.2 to 0.22, the distribution pattern of the laterally-averaged overall cooling effectiveness in the stream-wise direction alters significantly. When Bi equals to 0.022, the distribution of overall cooling effectiveness becomes more uniform in the stream-wise direction. But the value of laterally averaged overall cooling effectiveness at the downstream of film holes decreases about 4.2% compared to that of Bi=0.22. It is because that the convective cooling on the plate inner surface and the heat conduction in the solid consume part of the coolant become important in the case with a small Bi.

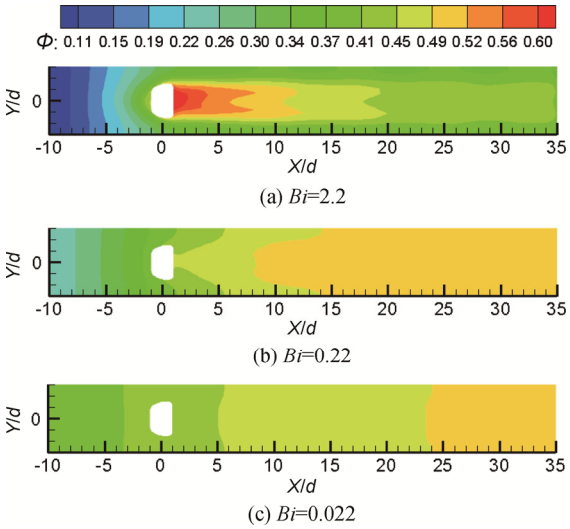

Fig. 7 Overall cooling effectiveness contour for different Bi

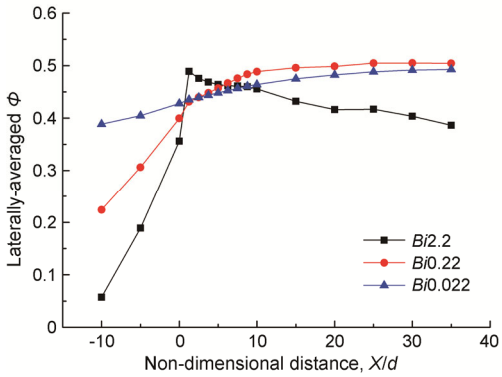

Fig. 8 Laterally-averaged overall cooling effectiveness distributions in the streamwise direction with different Bi

Fig. 9 shows the temperature contour at the centerline plane Y=0 around the film hole. It can be obviously seen that the temperature at the film hole inlet for Bi=0.022 is higher than those of the other two cases. As Bi decreases from 2.2 to 0.022, the coolant temperature at the film hole inlet changes from 304 K to 308 K. At the same

time, the coolant ejected temperature changes from about 310 K to about 316 K. Note that, under the same coolant inlet boundary condition, if the cooling potential of the coolants is less consumed by the convective cooling on the plate inner surface, the lower temperature of the coolant at the film hole inlet and outlet and thus a better film cooling effect can be obtained. With the decrease of Biot number, the proportion of impingement cooling effects is increased and the proportion of film cooling effects is accordingly decreased. For a specific combine cooling scheme and a given *BR*, there is an appropriate Biot number, which makes the coolant potential can be reasonably allocated to the internal and the external cooling to achieve the optimal overall cooling effectiveness.

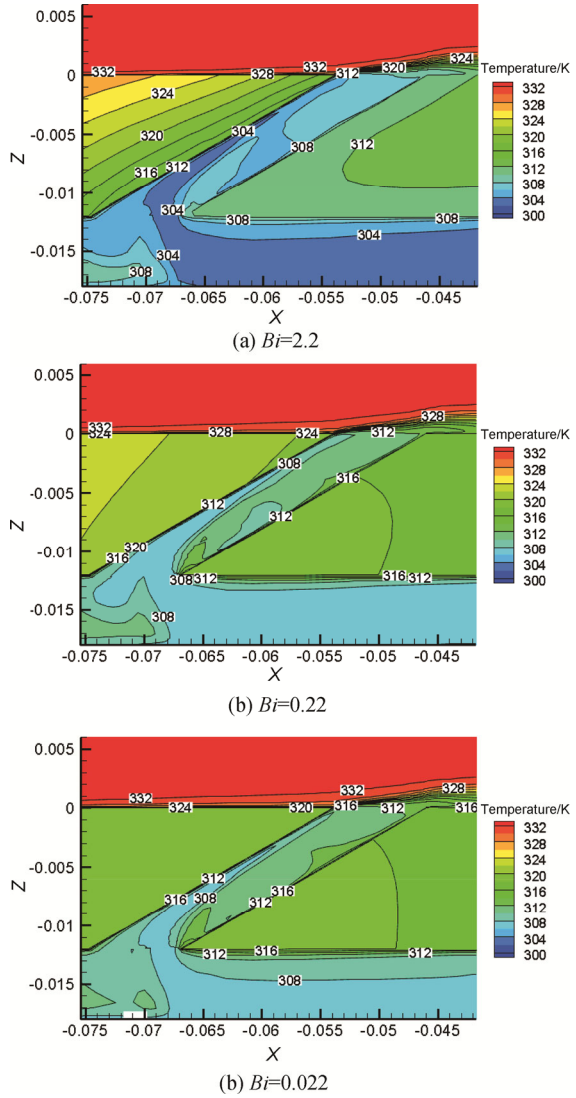

(a) *Bi*=2.2

(b) *Bi*=0.22

(b) *Bi*=0.022

Fig. 9 Temperature Contour in the film hole for different *Bi*

Figs. 10 and 11 show the flow streamlines at the centerline plane *Y*=0 of the impingement jet holes and the film hole for different *Bi*. The coolant passes through the impingement cooling holes, then flows into the film cooling hole. For the "jetting flow" discharges through the impingement hole, there are several vortexes occurring near to the target surface due to the deflection between the cross flow and the jet flow from the impingement holes. In addition, the coolant flows into the film cooling hole from two directions and forms a line when these two airflows encounter in the film cooling hole. Two vortexes are formed at different side of the encounter line. One is near to the exit of the film cooling hole and the other is located near to the leeward side of the film cooling hole inlet. By comparison, it seems that the flow structures in the impingement chamber and in the film cooling hole change little. It means that *Bi* has less influence on the internal and external flow structures.

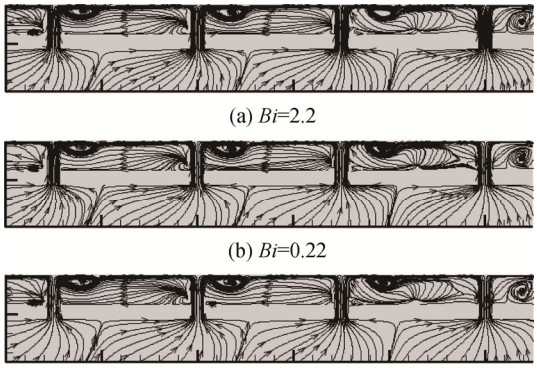

(a) *Bi*=2.2

(b) *Bi*=0.22

(c) *Bi*=0.022

Fig. 10 Streamlines in the jet holes for different *Bi*

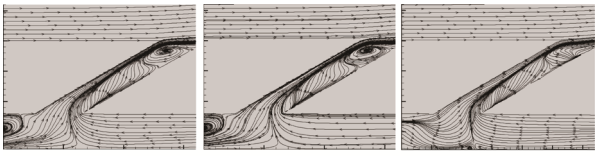

(a) *Bi*=2.2 (b) *Bi*=0.22 (c) *Bi*=0.022

Fig. 11 Streamlines in the film cooling hole for different *Bi*

4.2 Effects of blowing ratio

For a given Biot number, blowing ratio will impacts the overall cooling effectiveness, local convective heat transfer coefficient, temperature and flow flied. The metal's thermal conductivity is specified as 11 W/(m·K) and the corresponding *Bi* changes slightly from 0.22 at the blowing ratios of *BR*=0.5, 1.0, 1.5, 2.0, 2.5 and 3.0.

The overall cooling effectiveness on the wall surface of the main flow side for the fan-shaped film cooling hole configuration at all blowing ratios investigated are shown in Fig. 12. It can be seen that the overall cooling effectiveness is higher at the downstream region of the hole than that at the upstream region at either blowing ratio. With the increase of the blowing ratio, the region

with high overall cooling effectiveness is gradually enlarged, and the uniformity in the lateral direction of overall cooling effectiveness is also increased away from the film cooling hole exit.

Fig. 13 shows the stream-wise distributions of the laterally-averaged overall cooling effectiveness at different blowing ratios. In spite of different blowing ratios, the profiles of the laterally-averaged overall cooling effectiveness along the stream-wise direction are similar. The laterally-averaged overall cooling effectiveness is increased markedly from X/d=−10 to X/d=0, then slowly increased in the downstream region of the film cooling hole from X/d=0 to X/d=10, and increased to a nearly constant value from X/d=10 to X/d=35. But with the increase of blowing ratio, the improvement amplitude of the laterally-averaged overall cooling effectiveness is accordingly reduced. Moreover, the maximum values of the laterally-averaged overall cooling effectiveness differ a lot at different blowing ratios. The case of BR=0.5 exhibits a maximum value of about 0.33, but the case of BR=2.0 yields a maximum value of about 0.64. With the blowing ratio increasing from 2.0 to 3.0, the laterally-averaged overall cooling effectiveness downstream the film cooling hole changes little. That means that an optimal blowing ratio exists to obtain a highest overall cooling effectiveness for a specified cooling scheme.

The local convective heat transfer coefficient (h_f) distributions at the wall surface of the main flow side at different blowing ratios are presented respectively in

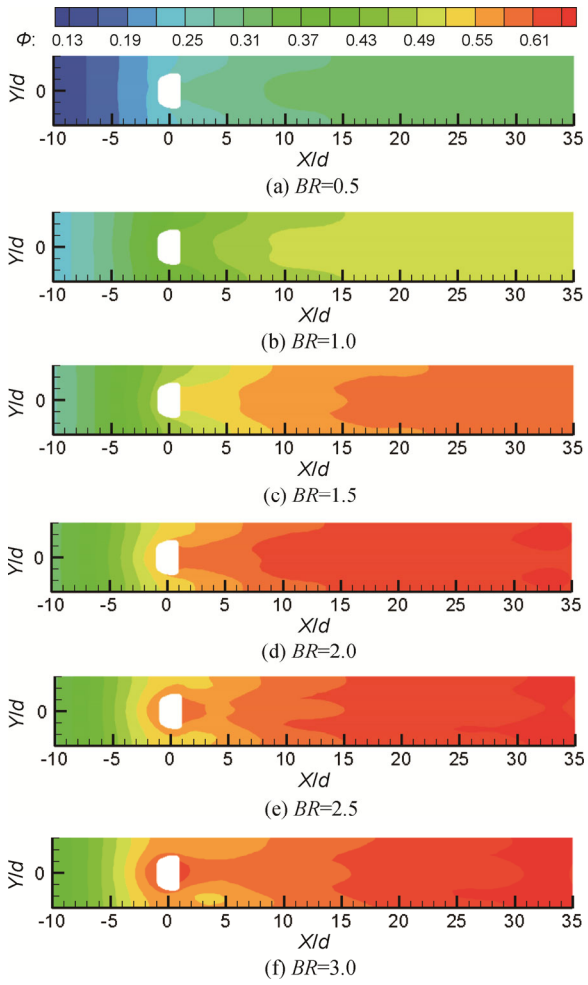

Fig. 12 Overall cooling effectiveness distributions over the wall surface of the main flow at different BR

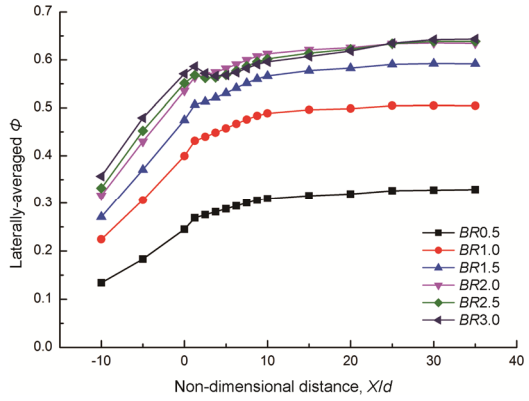

Fig. 13 Laterally-averaged overall cooling effectiveness in the stream-wise direction at different BR

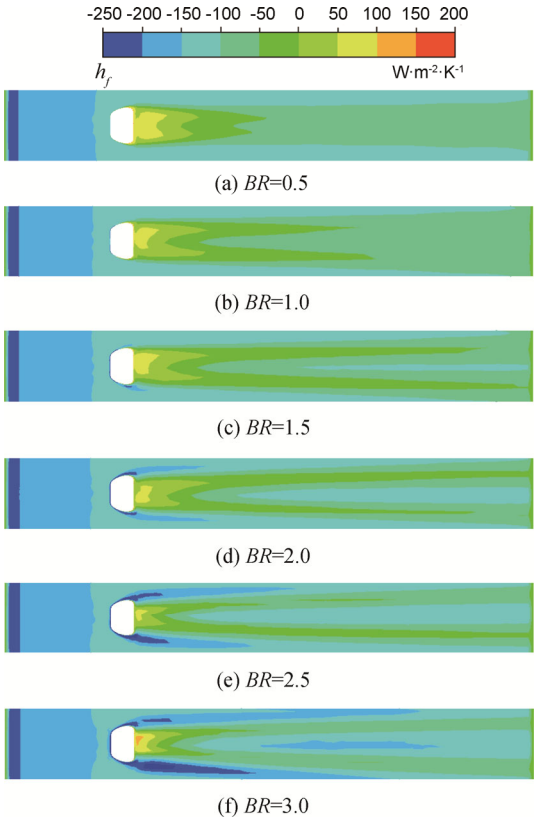

Fig. 14 Contours of the local convective heat transfer coefficient at the wall surface of the main flow side at different BR

Fig. 14. A negative h_f means that the main flow heats the film cooling plate, whereas a positive h_f means the film cooling plate heats the main flow. It is clearly shown that the flat plat heats the mixture of hot gas and coolant in the region downstream the film cooling hole where the value of h_f is positive. When the blowing ratio increases from 0.5 to 3.0, the area of the region with positive h_f reduces rapidly. Because more coolants are lifted off away from the wall of the main flow side at a higher blowing ratio, the values of h_f at the center line downstream the film hole decrease from positive to negative. Furthermore, the absolute value of h_f at the same location increases in the region with negative h_f especially at the two sides of the film cooling hole. Therefore, the increasing blowing ratio can enhance the heat transfer from the main flow to the film cooling plate.

Fig. 15 shows the local convective heat transfer coefficient (h_c) distributions on the target surface of the coolant side at different blowing ratios. It is obvious that with the increase of the blowing ratio, the impingement heat transfer performance is enhanced because of the increase of the impingement Reynolds number Re_i. The impingement Reynolds number is augmented from 1850 to 11100 corresponding to BR changes from 0.5 to 3.0.

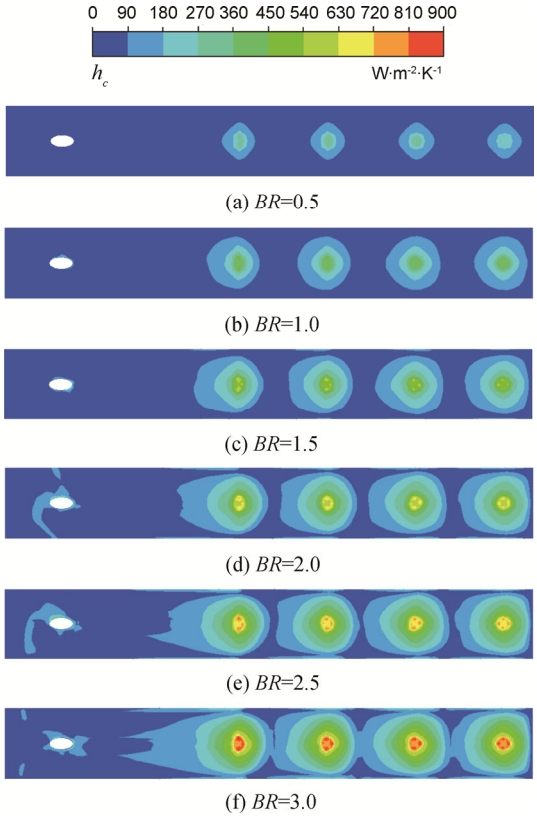

Fig. 15 Distributions of local convective heat transfer coefficient at the target surface at different BR

Besides, the influence of the cross-flow becomes stronger with the increase of the blowing ratio.

Fig. 16 shows the temperature contours at centerline plane Y=0 in the film hole at different blowing ratios. It can be seen that with the increasing of blowing ratio, the coolant temperatures at inlet and exit of the film cooling hole are reduced. The temperature of the film cooling plate near the film cooling hole is also decreased. The heat flux increases by 150% when the blowing ratio enhances from 0.5 to 3.0. So the more remarkable increase of the coolant mass flow rate counteracts the effects of the higher impingement heat transfer performance on the temperature of the coolant at high blowing ratio. In addition, there is a region with low temperature coolant in the film hole because the coolant is bended to leeward side of the film cooling hole. This low temperature region may be caused by the high velocity of the coolant in the film hole.

2D stream trances are plotted at the centerline cross plane in the film cooling hole and coolant chamber in order to investigate the impacts of blowing ratios, as shown in Figs. 17–18. Note that the increase from 0.5 to 3.0 of blowing ratio brings a decrease on the size of the vortex in the coolant chamber caused by the interaction between jet flow and cross flow. The locations of the vortex slightly move away from the impinging jet flow to the downstream location because of the jet flow becoming stronger under higher BR condition. For the film cooling, it can be seen that the vortex near the film hole exit is formed and grows up to occupy more and more the flow area of the film cooling hole with the blowing ratios changing from 0.5 to 1.5. But the vortex near the film hole exit disappears under BR=2.0, then occurs again at BR=2.5, and enlarges at BR=3.0. Hence, the flow fields are closely related to the blowing ratio in the coolant chamber and especially in the film cooling hole.

The surface streamline and the contours of the vortex intensity in X axis at the plane located at X/d=5 (the location of the film hole exit is X/d=0) are also illustrated in Fig. 19. The vortex intensity in X axis is defined by the following equation:

$$\omega_X = \frac{\partial w}{\partial y} - \frac{\partial v}{\partial z} \tag{6}$$

The change trend of the flow field downstream film hole varying with BR is similar with that at the adiabatic condition. A pair of vortex is generated by the cooling stream ejected from the film cooling hole. The scale of the vortex pair grows up with the blowing ratio increasing from 0.5 to 3.0. And this vortex pair is lifted off away from the wall surface since BR=2.0 which decreases the value of the film cooling effectiveness at high blowing ratios.

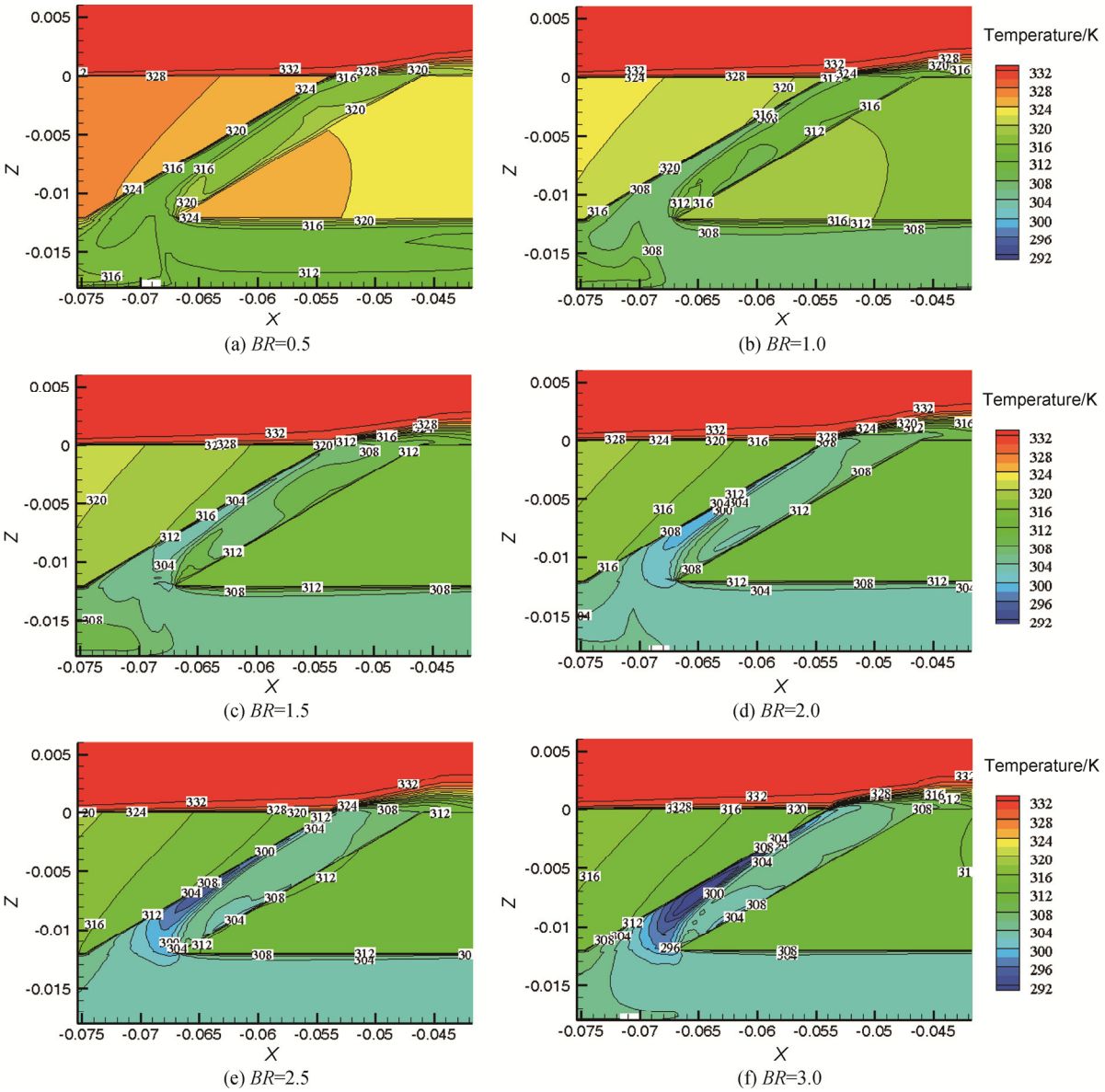

(a) *BR*=0.5 (b) *BR*=1.0

(c) *BR*=1.5 (d) *BR*=2.0

(e) *BR*=2.5 (f) *BR*=3.0

Fig. 16 Temperature contour in the film hole at different *BR*

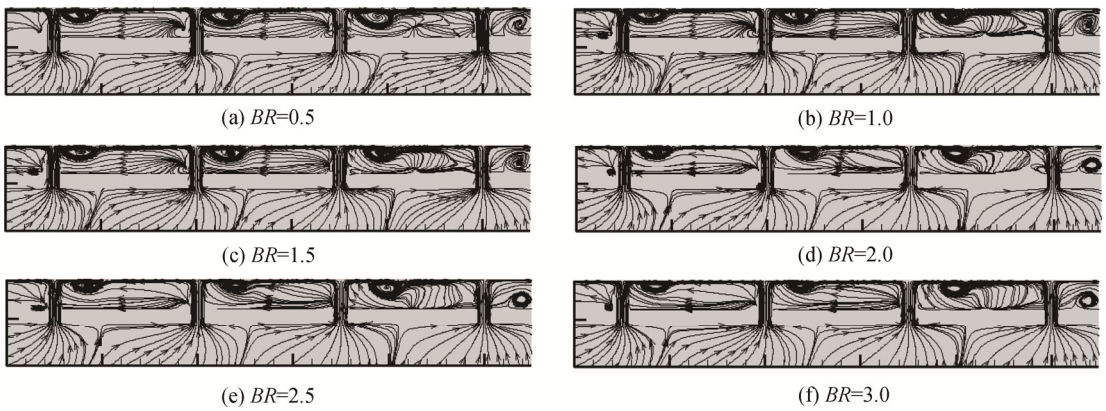

(a) *BR*=0.5 (b) *BR*=1.0

(c) *BR*=1.5 (d) *BR*=2.0

(e) *BR*=2.5 (f) *BR*=3.0

Fig. 17 Streamlines at *Y*=0 in coolant chamber at different *BR*

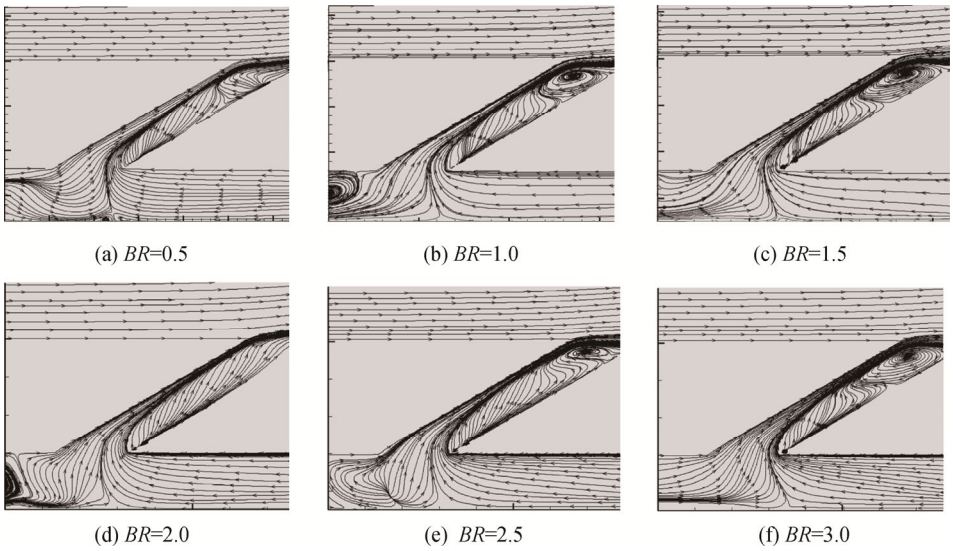

Fig. 18 Streamlines at Y=0 in the film cooling hole at different BR

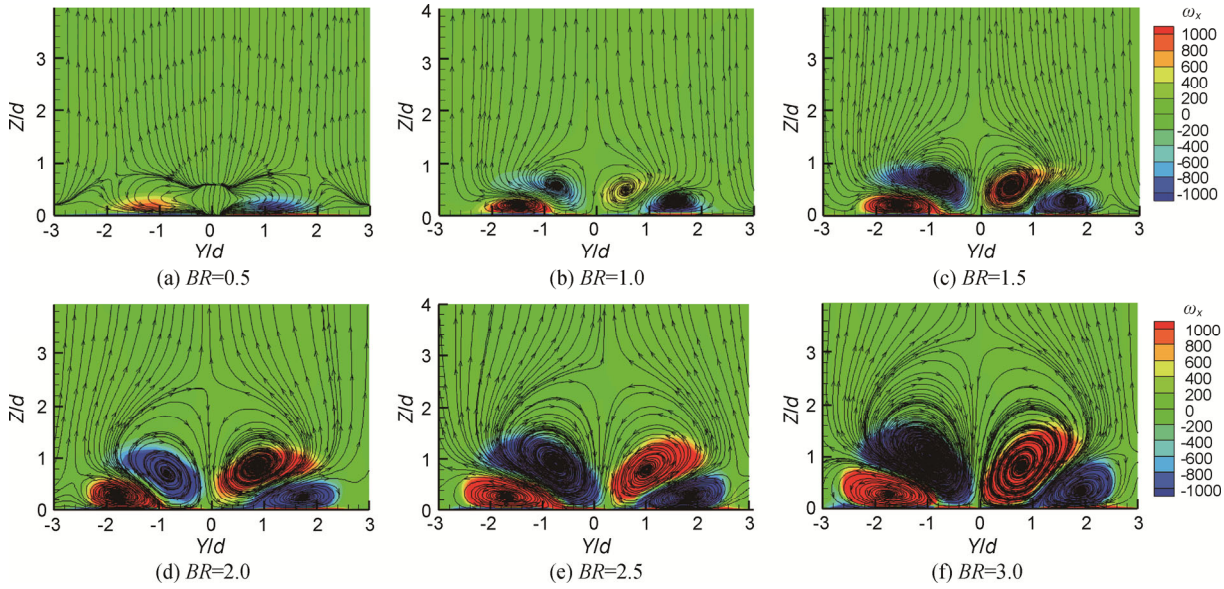

Fig. 19 Streamlines and vortex intensity in X axis at plane X/d=5 downstream the film hole at different BR

4.3 Effects of film hole shape

Film cooling hole geometry is an important parameter for the cooling performance. For a given blowing ratio, the film cooling hole geometry will impact the film cooling effectiveness, temperature field and the flow structure of ejected coolant from the cooling hole. Fan-shaped hole shows a better overall performance, especially at high blowing ratios, when compared to the standard cylindrical film cooling hole. So in this section, the conjugate heat transfer performances of the flat plate with two types of film cooling hole shapes are studied and compared. The cases of blowing ratio BR=0.5, 1.0, 1.5, 2.0, 2.5 and 3.0 are chosen for the comparisons between the cylindrical hole and fan-shaped hole.

The comparison of the distributions of laterally-averaged overall cooling effectiveness on the wall surface of the main flow side between the two typical film hole configurations are shown in Fig. 20. The fan-shaped hole demonstrates the higher overall cooling effectiveness at different blowing ratios. Obviously, the lateral-averaged Φ value increases near the "Impingement outlet" (i.e., the downstream of X/d>10) and it may be caused by the enhancement of inner heat transfer on the interface of the coolant side owing to the impingement cooling. But the trend of the laterally-averaged Φ curves exhibits a little different especially for the region

near the film hole exit for the combined cooling configures with various film hole geometry. For the cases with the cylinder-shaped film hole, the laterally-averaged overall cooling effectiveness reduces firstly and rises rapidly from the location X/d=2.5 at the blowing ratio BR=1.5, 2.0 and 2.5. For the cases with the fan shaped film hole, the similar trend only occurs at the blowing ratio BR=2.5. And the location of the laterally-averaged overall cooling effectiveness turning point is X/d= 2 which is a little close to the film hole exit. The distributions of the laterally averaged Φ for the plate with fan-shaped film holes are more uniform in the stream-wise direction than those for the plate with cylindrical holes.

At the blowing ratio of 0.5, the maximum laterally averaged Φ values of the plate with cylindrical film holes are near to that of the plate with fan-shaped holes. For the case with the cylinder film hole, with the blowing ratio increasing from 0.5 to 2.5, the improvement in the laterally averaged Φ is continuous. For the case with the fan-shaped film hole, the laterally averaged Φ changes little when the blowing ratio increases from 2.0 to 2.5. It seems that the influences of the impingement cooling to the overall cooling effectiveness depend on the geometry of the film hole. The improvements introduced by the impingement cooling are a little more distinct for the plate with cylindrical film holes. But with the BR increasing, the maximum value of the overall cooling effectiveness for different film hole shape trends to reach the same value.

Fig. 21 shows the local convective heat transfer coefficient (h_c) distributions on the target surface of the coolant side for the cases with cylindrical film cooling hole at different blowing ratios. Compared with those

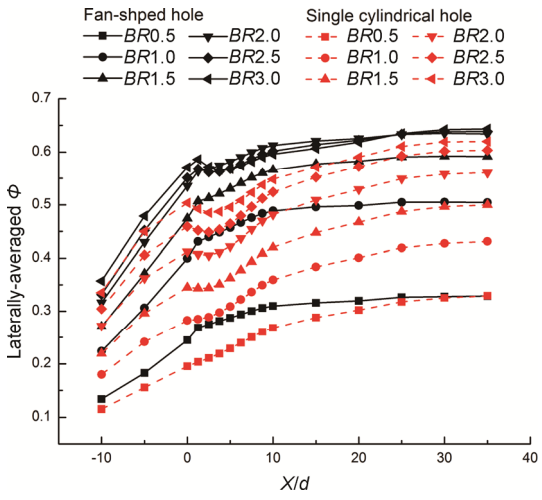

Fig. 20 Streamwise distributions of laterally-averaged Φ for cylindrical and fan-shaped film cooling holes

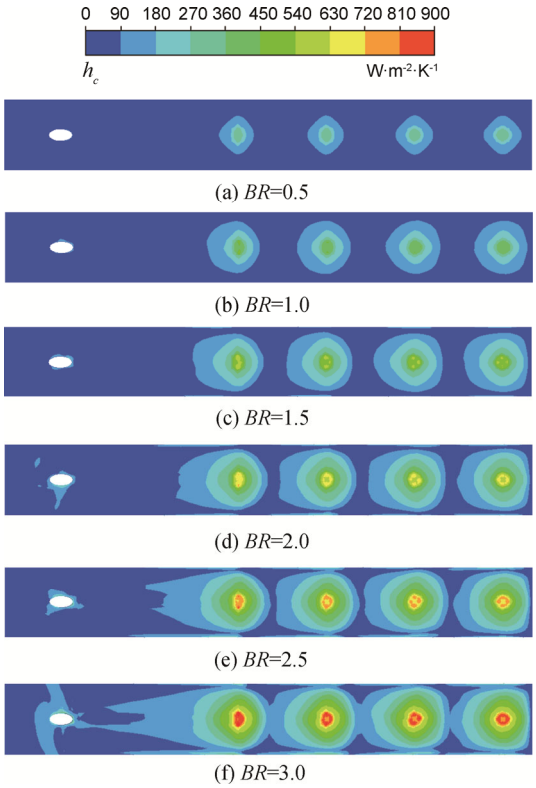

Fig. 21 Distributions of local convective heat transfer coefficients at the target surface with cylindrical film cooling hole at different BR

with the fan-shaped film cooling hole in Fig. 15 the distributions of the heat transfer coefficient (h_c) for the scheme with cylinder film cooling hole are similar. It seems that under the condition with the same Re_i, the film cooling hole shape imposes slight effect on the impingement cooling.

Fig. 22 gives the temperature contours at the centerline plane Y=0 in the cylindrical film cooling hole and the region near the film hole at different blowing ratios. The coolant temperature in the coolant chamber for the cylindrical film cooling hole case is the same to that for the fan-shaped film cooling hole case, which means the heat flux transferred by impinging cooling to the coolant is similar for different shapes of film hole.

The surface streamlines and the contours of the vortex intensity in X axis at the downstream plane X/d=5 are plotted at different blowing ratios for the cases with cylindrical film cooling hole, as shown in Fig. 23. Apparently, the kidney-shaped vortex pair dominates the flow field. And the scale of this vortex pair grows up with the increase of BR, which finally reduces the film cooling effectiveness. The lower film cooling effectiveness for cylindrical film cooling hole would result in a more contribution by the internal impingement cooling to the overall cooling effectiveness with the increase of BR.

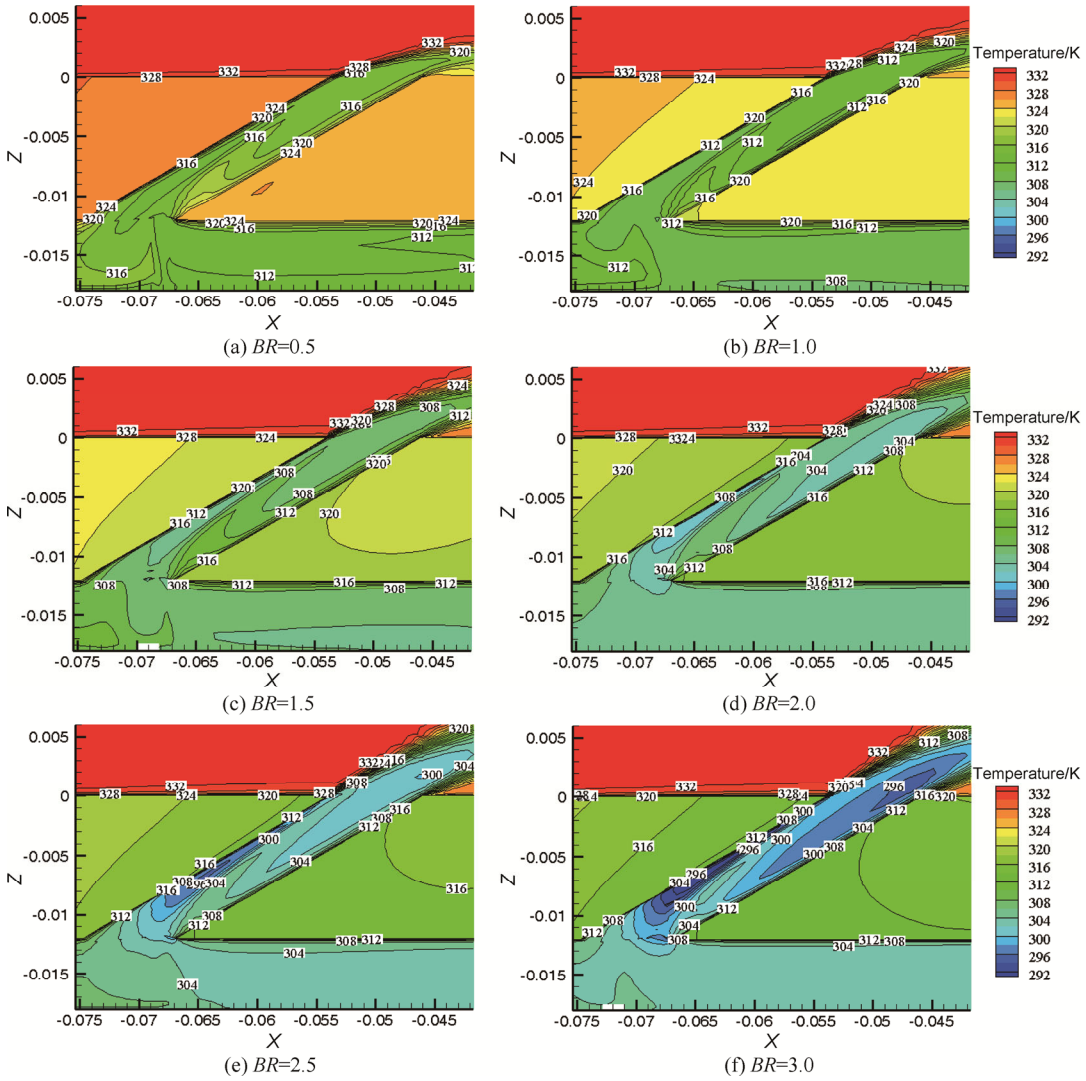

Fig. 22 Temperature contours in the circular film hole at different *BR*

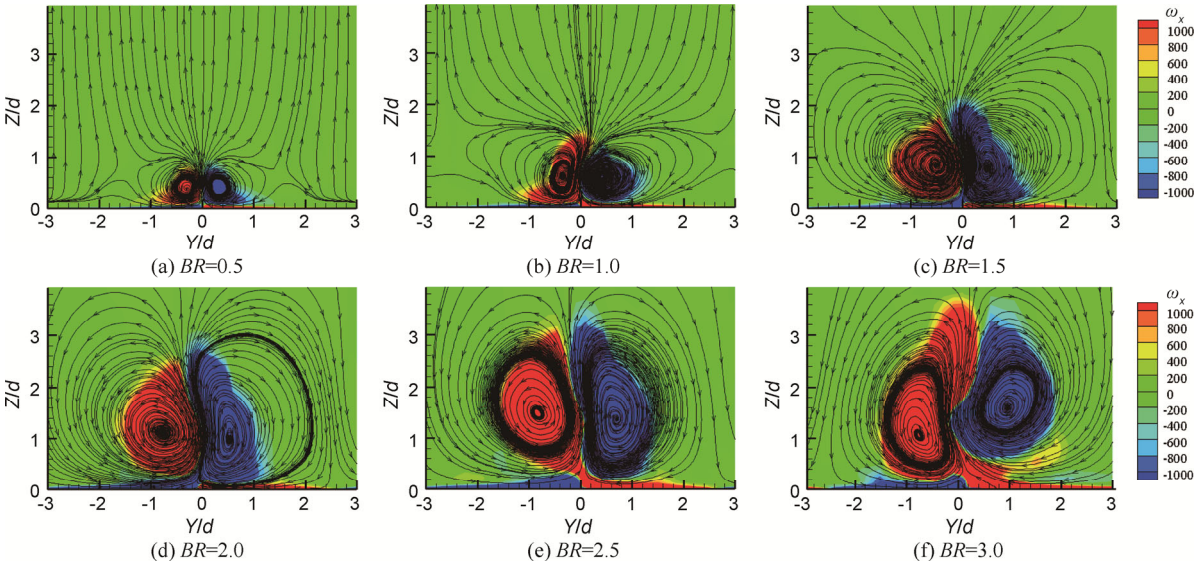

Fig. 23 Streamline in the plane *X*/*d*=5 downstream the cylindrical film cooling hole at different blowing ratios

4.4 Effects of impingement hole diameter

The effects of the impingement hole diameter on the overall cooling effectiveness, heat transfer on the both sides of the film cooling plate, the temperature of the coolant in the film hole and downstream flow fields are analyzed in this section. The diameters of the impingement hole are selected as 3 mm and 6 mm. The blowing ratios are both kept as BR=1.0.

The local overall cooling effectiveness contours and laterally-averaged overall cooling effectiveness with different diameters of the impingement hole are shown in Figs. 24–25. The overall cooling effectiveness reduces by 15% while the diameters of the jet hole change from 3 mm to 6 mm. At the same time, the impingement Reynolds number Re_i declines from 3700 to 1700, which results in a reduction of the convective heat transfer near the target wall and a higher wall temperature value in the side of the hot gas. It should be noticed that the overall cooling effectiveness tapers at the downstream location of the film hole. It reveals that the effect caused by the impingement is declined while the diameter of the hole increases. Hence the film cooling dominates the overall cooling effectiveness of the combined cooling. The overall cooling effectiveness decreases at the downstream location due to the reduction of the film cooling effectiveness.

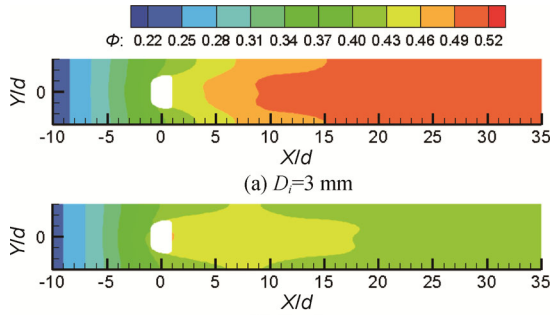

Fig. 24 Overall cooling effectiveness contours for different diameters of impingement hole

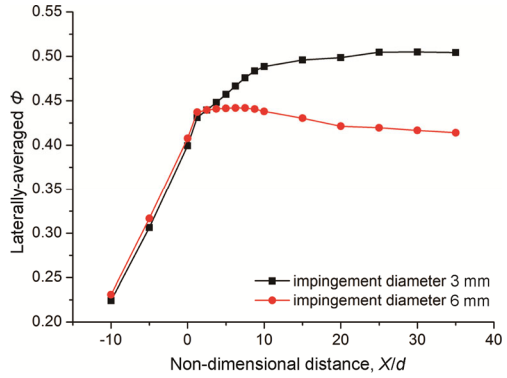

Fig. 25 Distribution curves of laterally-averaged overall cooling effectiveness for different diameters of impingement hole

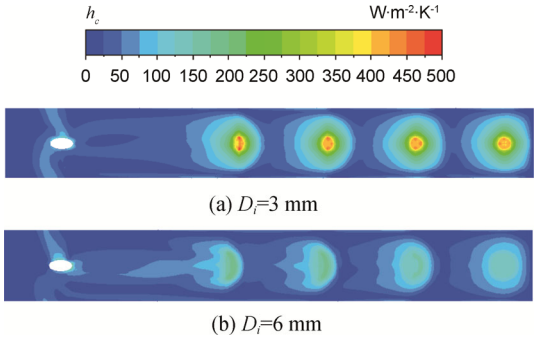

Fig. 26 Local heat transfer coefficient distribution on the target surface

The distributions of the local heat transfer coefficient of the target surface at the coolant side with different diameters of impingement holes are shown in Fig. 26. It can be seen that the local heat transfer coefficient of the jet core area is decreased by nearly 40% when the impingement hole diameter is enlarged. For the case with large impingement hole diameter, the jet velocity is reduced, and the shape of jet becomes easier to be changed. As shown in Fig. 26, the shape of the impingement core formed by the "jet flow" from the impingement hole becomes irregular by the influence of the cross flow. The changes of the core shape are more obvious due to the accumulation of the cross flow at the downstream location of the impingement holes. At the same time, because the impingement Reynolds number Re_i declines from 3700 to 1700, a reduction of the convective heat transfer coefficients results in a poor overall cooling effectiveness at the wall surface on the main flow side as shown in Fig. 24.

2D stream trances are plotted at the centerline cross plane in the film cooling hole and coolant chamber in order to investigate the impacts of film hole exit shape under different blowing ratios, as shown in Fig. 27. Due to the diameter increasing, the impingement Reynolds number Re_i declines. The influence imposed by the cross flow on the jet flow becomes strong.

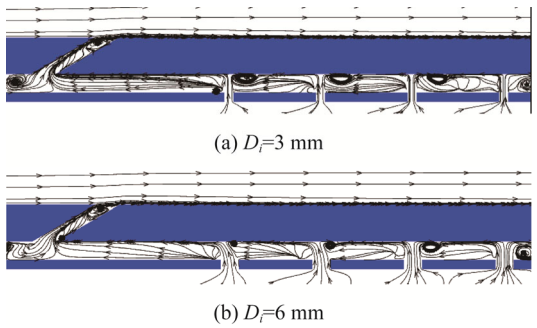

Fig. 27 Streamlines at central plane of film cooling hole for different diameters of the impingement hole

5. Conclusions

In this paper, conjugate heat transfer for a flat plate with a dual effect of film cooling and impingement cooling are investigated. The numerical results show the effect of Biot number, blowing ratios, film cooling hole shape and impingement hole diameter on the overall cooling effectiveness and the flow fields. Some major conclusions are concluded as follows:

(1) For a specific combined cooling scheme and a given *BR*, the Biot number (i.e. the thermal conductivity of the film cooling plate in present study) decides the contribution proportion of impingement cooling and film cooling to the overall cooling effectiveness. The cooling potential of the coolant should be reasonably allocated to the internal and the external cooling to achieve the optimal overall cooling effectiveness.

(2) The blowing ratio influences both the cooling performance of the impinging cooling and the film cooling. With the increase of the blowing ratio, the local convective heat transfer coefficient at the target surface for impinging cooling improves, but the coolant ejection from the film cooling hole trends to lift off and leads to a poor coolant coverage over the wall surface on the hot gas side. The improvement amplitude of the laterally-averaged overall cooling effectiveness is reduced with the increase of the blowing ratio.

(3) For the schemes with cylindrical and fan-shaped film cooling holes, the effects of the blowing ratio on the overall cooling effectiveness are different. But there is a maximum overall cooling effectiveness for a specific cooling scheme.

(4) At a given mass flow rate of coolant, the increase of the impingement hole diameter leads to the decrease of the impingement Reynolds number which causes the effect of the impingement on the overall cooling effectiveness to decline.

Acknowledgement

The authors wish to acknowledge the financial support from the National Natural Science Foundation of China under Grant No. 51776201 and the National Science Foundation of Tianjin under Grant No. 18JCQNJC07200.

References

[1] Kercher D.M., A film-cooling CFD bibliography: 1971–1996. International Journal of Rotating Machinery, 1998, 4: 61–72.

[2] Bunker R.S., A review of shaped hole turbine film cooling Technology. Journal of Heat Transfer, 2005, 127: 441–453.

[3] Han J.C., Dutta S., Ekkad S.V., Chapter 3 Turbine Film Cooling, Gas Turbine Heat Transfer and Cooling Technology, Second edition, CRC Press-Taylor & Francis Group, Boca Raton, Florida, ISBN: 978-1- 4398-5568-3, 2012.

[4] Ekkad S.V., Han J.C., A review of hole geometry and coolant density effect on film cooling. Frontiers in Heat and Mass Transfer, 2015, 6: 1–14.

[5] Goldstein R.J., Eckert E.R.G., Burggraf F., Effects of hole geometry and density on three- dimensional film cooling. International Journal of Heat & Mass Transfer, 1974, 17: 595–607.

[6] Sinha A.K, Film-cooling effectiveness downstream of a single row of holes with variable density ratio. Journal of Turbomachinery, 1991, 113: 442–449.

[7] Fric T.F, Vortical structure in the wake of a transverse jet. Journal of Fluid Mechanics, 1994, 279: 1–47.

[8] Schmidt D.L., Sen B., Bogard D.G, Film cooling with compound angle holes: adiabatic effectiveness. Journal of Turbomachinery, 1996, 118: 807–813.

[9] Thole K., Gritsch M., Schulz A., Wittig S, Flow field measurements for film-cooling holes with expanded exits. Journal of Turbomachinery, 1998, 120: V004T09A010.

[10] Brittingham R.A., Leylek J.H., A detailed analysis of film-cooling physics: part IV- compound angle injection with shaped holes. ASME Journal of Turbomachinery, 2000, 122: 113–121.

[11] Gao Z., Han J.C, Influence of film-hole shape and angle on showerhead film cooling using PSP technique. Journal of Heat Transfer, 2009, 131: 177–181.

[12] Bohn D., Ren J., Kusterer K., Conjugate heat Transfer analysis for film cooling configurations with different hole geometries. ASME Turbo Expo 2003: Turbine Technical Conference and Exposition, 2003, GT2003-38369.

[13] Silieti M., Kassab A.J., Divo E., Film cooling effectiveness: eomparison of adiabatic and conjugate heat Transfer CFD models. International Journal of Thermal Sciences, 2009, 48: 2237–2248.

[14] Liu J.J., Wang Z., Fu J.L. et al., Multi-Field coupling investigation of film cooling with different hole configuration. Proceedings of 11th International Symposium on Experimental and Computational Aerothermodynamics of Internal Flows, 2013, No. 39.

[15] Zhang C., Liu J.J., Wang Z., et al., The effects of the Biot number on the conjugate film cooling effectiveness under different blowing ratios. ASME Turbo Expo 2013: Turbine Technical Conference and Exposition, 2013, GT2013-94041.

[16] Gardon R., Akfirat J.C., Heat transfer between a flat plate and jets of air impinging on it. International Journal of Heat & Fluid Flow, 1962, 8: 1261–1272.

[17] Cooper D., Jackson D.C., Launder B.E. et al., Impingement jet studies for turbulent model assessment-I.

flow-field experiments. International Journal of Heat & Fluid Flow, 1993, 36: 2675–2684.

[18] Ashforth-Frost S., Flow visualization of semiconfined jet impingement. The Nottingham Trent University, Nottingham, U.K, 1994.

[19] Huang Y.Z., Ekkad S.V., Han J.C., Detailed heat transfer distributions under an array of orthogonal impinging jets. Journal of Thermophysics and Heat Transfer, 1998, 12(1): 73–79.

[20] Ball S.J., Near wall flow characteristics in jet impingement heat transfer. The Nottingham Trent University, Nottingham, U.K., 1998.

[21] Downs S.J., James E.H., Jet impingement heat transfer - a literature survey. ASME, Aiche, and Ans, 24th National Heat Transfer Conference and Exhibition, 1987, 87-H-35.

[22] Viskanta R., Heat transfer to impingement isothermal gas and flame jets. Experimental Thermal Fluid Science, 1993, 6: 111–134.

[23] Cho H.H., Rhee D.H., Kim B.G., Enhancement of film cooling performance using a shaped film cooling hole with compound angle injection. JSME International Journal, 2002, 44: 99–110.

[24] Goodro M., Park J., Ligrani P., et al., Effects of Mach number and Reynolds number on jet array impingement heat transfer. International Journal of Heat Mass Transfer, 2007, 50: 367–380.

[25] Goodro M., Park J., Ligrani P., et al., Effects of hole spacing on spatially-sesolved jet array impingement heat transfer. International Journal of Heat Mass Transfer, 2008, 51: 6243–6253.

[26] Goodro M., Ligrani P., Fox M., et al., Mach number, Reynolds number, jet spacing variations: full array of impinging jets. Journal of Thermophysics and Heat Transfer, 2010, 24: 133–144.

[27] Sweeney P.C., Rhodes J.F., An infrared technique for evaluating turbine airfoil cooling designs. Journal of Turbomachinery, 1999, 122: 1–10.

[28] Panda R.K., Prasad B.V.S.S.S., Conjugate heat transfer from a flat plate with combined impingement and film cooling. ASME Turbo Expo 2012: Turbine Technical Conference and Exposition, 2012, GT2012-68830.

[29] Panda R.K., Prasad B.V.S.S.S., Conjugate heat transfer from an impingement and film cooled flat plate. Journal of Thermophysics and Heat Transfer, 2014, 28: 647–666.

[30] Maikell J., Bogard D.G., Piggush J., Kohli A, Experimental simulation of a film cooled turbine blade leading edge including thermal barrier coating effects. ASME Journal of Turbomachinery, 2011, 133: 011014.

[31] Mouzon B.D., Terrell E.J., Albert J.E., et al., Net heat flux reduction and overall effectiveness for a turbine blade leading edge. ASME Turbo Expo 2005: Turbine Technical Conference and Exposition, 2005, GT2005-69002.

[32] Ravelli S., Dobrowolski L., Bogar D.G, Evaluating the effects of internal impingement cooling on a film cooled turbine blade leading edge. ASME Turbo Expo 2010: Turbine Technical Conference and Exposition, 2010, GT2010-23002.

[33] Nathan M.L., Dyson T.E., Bogard D.G., et al., Adiabatic and overall effectiveness for the showerhead film cooling of a turbine vane. Journal of Engineering for Gas Turbines and Power, 2014, 136: 031005-1–031005-9.

[34] Mensch A., Thole K.A., Overall effectiveness of a blade endwall with jet impingement and film cooling. Journal of Engineering for Gas Turbines and Power, 2014, 136: 031901-1–031901-10.

[35] Mensch A., Thole K.A., Craven B.A., Conjugate heat transfer measurements and predictions of a blade endwall with a thermal barrier coating. Journal of Engineering for Gas Turbines and Power, 2014, 136: 121003-1–121003-11.

[36] Mensch A., Thole K.A., Simulations of multiphase particle deposition on a gas turbine endwall with impingement and film cooling. ASME Journal of Turbomachinery, 2015, 137: 111002-1–111002-8.

[37] Mensch A., Overall Effectiveness of a blade endwall with jet impingement and film cooling. Journal of Engineering for Gas Turbines & Power, 2014, 136: 031901.

[38] Jung E.Y., Chung H., Choi S.M., et al., Conjugate heat transfer on full-coverage film cooling with array jet impingements with various Biot numbers. Experimental Thermal & Fluid Science, 2017, 83: 1–8.

[39] Zhang P., Investigation on film cooling and combined cooling using conjugate heat transfer method. The University of Chinese Academy of Sciences, Beijing, China, 2015. (in Chinese)

[40] Harrison K.L., Bogard D.G., Use of the adiabatic wall temperature in film cooling to predict wall heat flux and temperature. ASME Turbo Expo 2008: Turbine Technical Conference and Exposition, 2008, GT2008-51424.